

Evaluation of the Spectroscopic Performance of 3D CZT Drift Strip Detectors

N. Auricchio, E. Caroli, S. Del Sordo, L. Abbene, A. Buttacavoli, F. Principato, G. Gerardi, J. B. Stephen, M. Bettelli, N. Sarzi Amadè, S. Zanettini, A. Zappettini, N. Protti, S. Altieri and due2lab s.r.l.

Abstract— CdTe/CZT is an attractive and consolidated material with which to realize detectors with good efficiency and energy resolution, operating at room temperature and suitable for a large variety of applications such as medical imaging, nuclear security, and astrophysics. Right in this last field several spectro-imagers based on these CdTe/CZT detectors were mounted onboard space missions such as INTEGRAL, Swift, and NuSTAR for hard X and gamma-ray astrophysics. Much effort has been expended in the development of CZT spectroscopic imagers for obtaining sub-millimeter spatial resolution in three dimensions (3D) and high energy resolution up to 1 MeV. The motivations are mainly related to the possibility to perform simultaneous measurements of energy, timing, and 3D positioning of X and gamma rays. This kind of 3D detector is particularly suitable to realize scattering polarimeters and Advanced Compton detectors. In this paper, we present the performance of high-resolution CZT drift strip detectors, recently realized at IMEM-CNR (Parma, Italy) in collaboration with due2lab company (Scandiano, Italy). The detectors are operated in the Planar Transverse Field (PTF) configuration, in which photons hit the detector orthogonally to the direction of the electric field established between the two electrodes, as well as in the standard configuration. They are able to determine the 2D position thanks to the strips deposited on electrodes orthogonally, while the third coordinate is derived from the Cathode/Anode ratio and/or drift time. We report the experimental results in terms of energy resolution, peak-to-valley ratio, threshold, and gain, as well as charge collection efficiency for 2 different samples and several energies of calibration. We also report the results obtained by using a novel correction technique based on the analysis of collected-induced charge pulses from anode and drift strips.

Index Terms— X-ray and Gamma-ray detectors, Spectroscopy, Semiconductor radiation detectors

I. INTRODUCTION

Missions for hard X- and Gamma-ray astrophysics in the keV to MeV band require advanced instrumentation in

Manuscript received December 15, 2021. This work was supported by the Italian Space Agency.

N. Auricchio, E. Caroli and J. B. Stephen are with the INAF - OAS Bologna, via Gobetti 93/3, 40129, Bologna, Italy (telephone: +390516398779, e-mail: natalia.auricchio@inaf.it).

S. Del Sordo is with the INAF/IASF Palermo, via Ugo La Malfa 153, 90146, Palermo, Italy.

L. Abbene, A. Buttacavoli, F. Principato and G. Gerardi are with the Department of Physics and Chemistry (DiFC) - E. Segrè, University of Palermo, Viale delle Scienze, Edificio 18, Palermo, 90128, Italy.

M. Bettelli, N. Sarzi Amadè, S. Zanettini and A. Zappettini are with IMEM/CNR, Parco Area delle Scienze 37/A, 43100, Parma, Italy.

N. Protti and S. Altieri are with the Department of Physics, University of Pavia, via Agostino Bassi 6, Pavia, 27100, and PV-INFN, Italy.

due2lab s.r.l, Via Paolo Borsellino 2, 42019, Scandiano, Italy.

terms of both spectral and imaging capabilities of the detectors, which must have high efficiency, energy resolution of a few keV, and the capability of position sensitivity in three dimensions (3D). Room-temperature semiconductor detectors such as CdZnTe (CZT) and CdTe [1], [2] are good candidates for this kind of instrumentation even if their major drawback is the ineffective charge collection within the detector, especially for the holes, which affect and degrade the detector spectral performance.

II. AIM OF THE WORK

The reasons that drive us to realize 3D detectors are mainly due to the perspective to perform measurements of energy, timing, and 3D positioning of X and gamma rays at the same time. In particular, 3D detectors are suitable for scattering polarimetry in hard X and gamma-ray range, therefore this kind of sensors can fulfill the challenging requirements of new instrumentation for high energy astronomy, like focusing telescopes based on broadband Laue lens and advanced Compton instruments. In addition, they can efficiently answer the needs of different space mission scenarios: from instruments for single satellites to constellations of nanosatellites thanks to their high modularity.

The present work aims to report a complete characterization of the spectroscopic performance of new 3D CZT drift strip detectors, in both standard and Planar Transverse Field (PTF) geometries.

III. ADVANTAGES OF CdTe/CdZnTe

The performances of detectors based on CdTe/CdZnTe strongly depend on the peculiar intrinsic properties of this material, reported in the table below:

TABLE I. CdTe/CZT CHARACTERISTICS

Properties	Effect
Efficiency due to high Z (48, 52) high density (6.20 g cm ⁻³)	High absorption
Low pair-creation energy (4.43 eV) + Good e- transport properties performances ($\mu\tau$) _e ~ 10 ⁻³ ÷ 10 ⁻² cm ² /V	Good spectroscopic
Low bandgap (1.44 eV), high resistivity > 10 ⁹ Ω.cm	Low noise at room temperature
Modular systems	Array/matrix
Imaging capability	3D position

IV. 3D DETECTORS APPROACH

A very productive collaboration was established with the Technical University of Denmark that developed the so-called Drift Strip Method (DSM), less sensitive to the hole collection, to reduce the effects caused by their trapping, which leads to a degradation in the energy resolution. In addition, DTU developed a new approach to improve the detector spatial resolution due to the readout of the drift strip.

In the framework of a project funded by the Italian Space Agency, we have segmented the detectors on both sides allowing a few readout channels (~ 100) to obtain a sensor segmentation equivalent to ~ 16000 voxels. It is worth noticing that a low bias voltage (300-400 V/ 5 mm), a low energy threshold and a good efficiency at high energy from 5-10 keV to 700-800 keV represent further advantages.

A. Double-Sided Drift Strip Detector

The anode structure implements the drift strip technique [3], [4], employing 3 drift strips that separate the anode readout strips. The drift strip detector consists of cathodic and anodic strips orthogonally deposited on the sides of the crystal, giving a two-dimensional position resolution, while the depth information can be derived from the cathode/anode ratio or the drift time. The drift cell consists of 4 drift strip electrodes, biased negatively by a voltage divider, to focalize the charge electrons on the anode readout strip surrounded on each side by 2 drift strips in which the central one is shared with two consecutive anodes. The drift strips are ac-coupled together in two groups of left (DL) and right (DR) strips and connected to their respective preamplifier through a decoupling capacitor. The following scheme describes the layout of the new DSDDS detector.

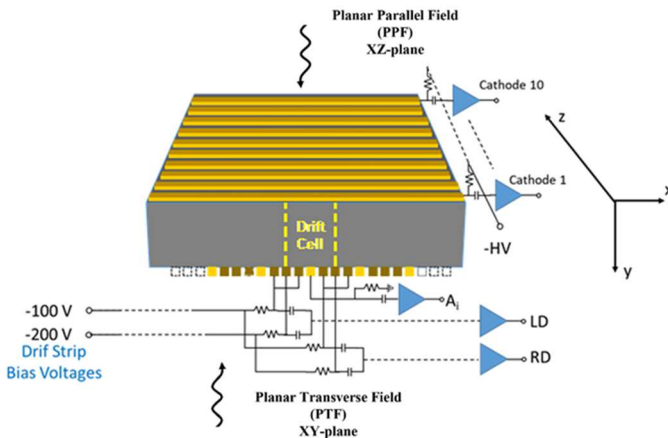


Fig. 1. Drawing of the new DSDDS detector.

We have illuminated the detector both in the standard configuration (Planar Parallel Field,) typically through the cathode, and in an irradiation configuration, named Planar transverse field PTF, in which the direction of the incoming photons is perpendicular to the electrical field, decoupling the photon absorption thickness from the charge collection efficiency. Then, this configuration allows the photon absorption thickness to be increased up to a few centimeters without increasing the charge collection distance, avoiding severe spectroscopic performance degradation.

V. DETECTORS AND ELECTRONICS

The detectors were fabricated at IMEM-CNR from CZT crystals grown by Redlen with the traveling heater method (THM). The dimensions of the CZT crystals are $19.44 \times 19.44 \times 6$ mm³. In particular, the detectors were re-fabricated after electrode removal and surface treatments. The CZT crystals grown at the Redlen company (website: <http://redlen.ca>) are spectroscopic grade with excellent charge transport properties (mobility-lifetime products of electrons $\mu_e \tau_e$ greater than 10^{-2} cm²/V). The layout of the anode and cathode is characterized by strip electrodes with the following configuration:

- Anode side, divided into 48 gold strips
 - pitch = 0.4 mm, strip width = 0.15 mm, inter-strip gap = 0.25 mm
- Due to this configuration, the 12 collecting strips have a pitch of 1.6 mm.
- Cathode side, divided into 10 gold strips orthogonal to the anode strips
 - pitch = 2 mm, strip with = 1.9 mm, inter-strip gap = 0.1 mm.

The collecting anode strips, the drift strips, and the cathode strips were AC coupled to hybrid Charge Sensitive Preamplifiers (ENC 100 electrons) developed at DiFC of the University of Palermo (Italy) [5]. The cathode strips are biased negatively at -350V. The voltage divider supplies each drift strip with an optimized bias, while the anode strips are held at ground potential. Fig. 2 shows the anode side and the detail of the cathode bonding.

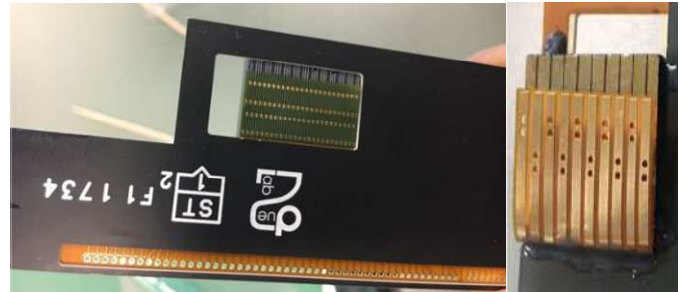


Fig. 2. Picture of the anode side (left); photo of the cathode bonding in detail (right).

VI. ELECTRICAL CHARACTERIZATION

The electrical characterization, performed at IMEM, on 4 detectors shows a very low mean surface leakage current and 48 strips homogeneous one each other, as reported in Table II and Fig. 3.

TABLE II. MEAN VALUE AT ± 50 V OF THE INTER-STRIP LEAKAGE CURRENT

Detector	Inter-strip leakage current: mean value at ± 50 V
D1	1.49 nA
D2	0.98 nA
D3	0.85 nA
D4	1.34 nA

The measured bulk leakage current is less than 1.4 nA at -600 V.

The electrical characterization, performed on all the realized samples, allows us to validate a reproducible technologic fabrication technique on a large area (~20 mm x 20 mm) and confirm the quality of the bonding process, that is an extremely challenging step of the project, as each strip is electrically connected through conductive glue to the gold lines insulated by Kapton film.



Fig. 3. The surface current of the detector D3 is acquired after the bonding process.

VII. EXPERIMENTAL SETUP

The 3D CZT crystal is mounted and bonded to the support I/F, provided by due2lab s.r.l., with the AFEE board, in which all channels are AC coupled to the custom CSPs (see Fig 4) and contained in a light-tight box, which is equipped with an XY micrometric tablet to perform scans in the PTF configuration, as illustrated in Fig. 5, irradiating the sensors with a collimated source even if the collimation is poor at high energy.

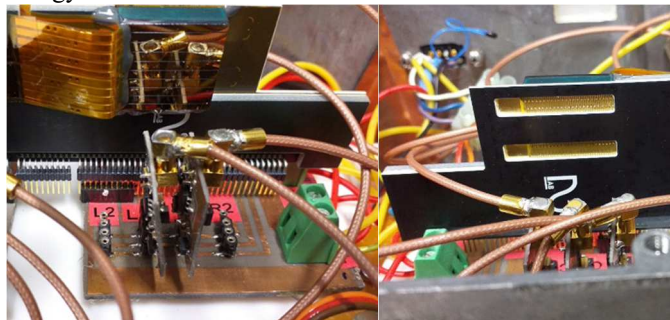


Fig. 4. Support interface with the Analog Front End Electronics.

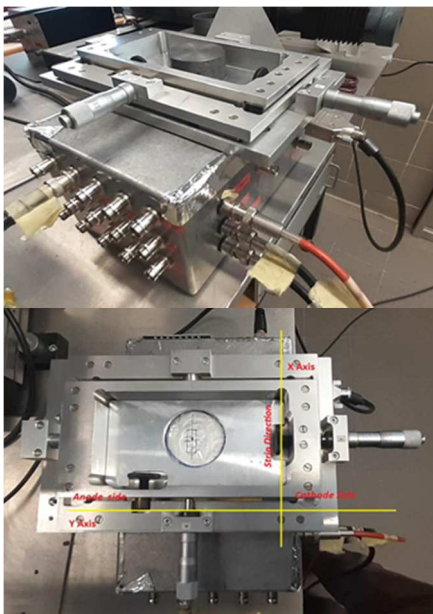


Fig. 5. Picture of the light-tight box containing the detector and the CSP.

VIII. DETECTOR CHARACTERIZATION

We have studied the transport properties of four detectors by measuring the $\mu\tau$ product as well as by determining their response to irradiation with different calibration sources like ^{241}Am , ^{57}Co , ^{109}Cd , and ^{137}Cs , in both PTF and standard configurations.

We present the results of this spectroscopic characterization focusing on the energy resolution, charge collection efficiency, peak to ratio valley, and threshold. In addition, we report the results of the irradiation in PTF geometry at different positions with respect to the cathode.

Firstly, by using the experimental set-up previously described we have determined the bias voltage increasing separately the bulk, left-right, and central drift strip voltages and then with a voltage divider to obtain the best compromise between the CCE and energy resolution (see Fig. 6 and 7).

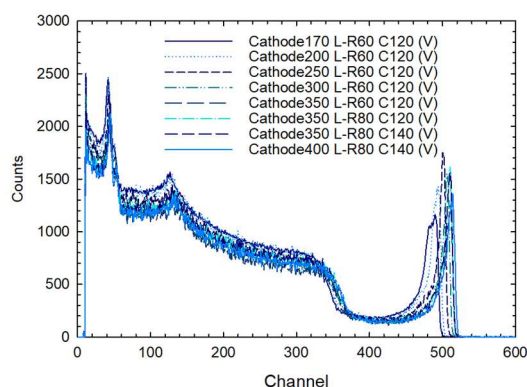


Fig. 6. ^{137}Cs Spectra of the detector D1 acquired at several bias voltages of the bulk, left & right drift strip, and central drift strip.

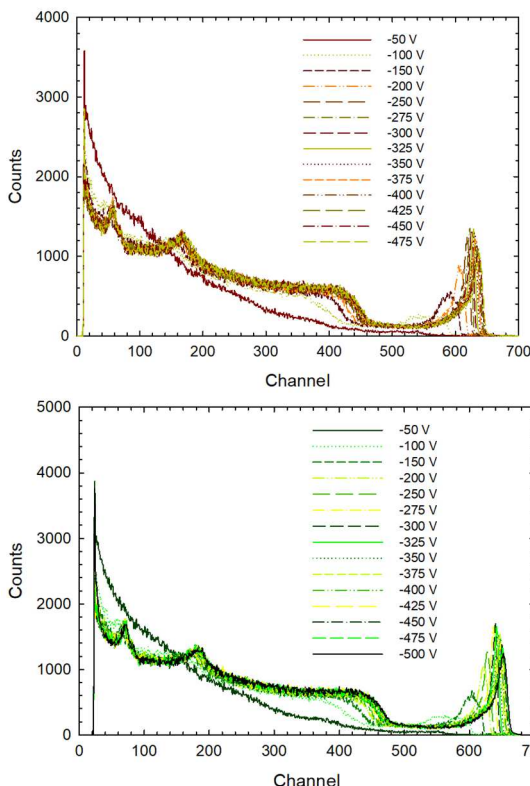


Fig. 7. ^{137}Cs Spectra of the detector D2 (top) and D3 (bottom) as a function of the bias voltage provided to the drift strips by a voltage divider.

A. Detector characterization in PPF and PTF

The comparison of the spectra recorded by irradiating the 4 detectors in the standard common geometry (PPF) at different energies with ^{241}Am , ^{109}Cd , ^{57}Co , and ^{137}Cs is reported in the following figure.

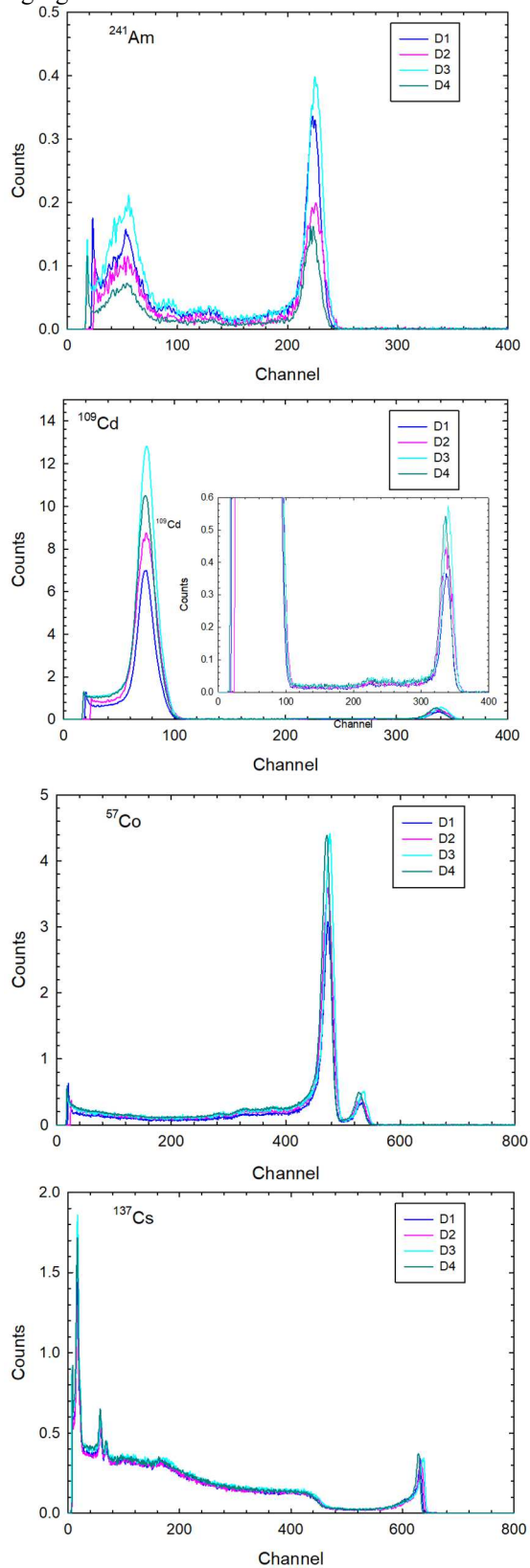


Fig. 8. Spectra acquired irradiating the 4 detectors in PPF.

All the detectors show the same CCE, confirmed in the PTF configuration illuminating them at the same energies and in three positions between the electrodes: near the anode, in the center, and near the cathode. Fig. 9 reports the relative spectra.

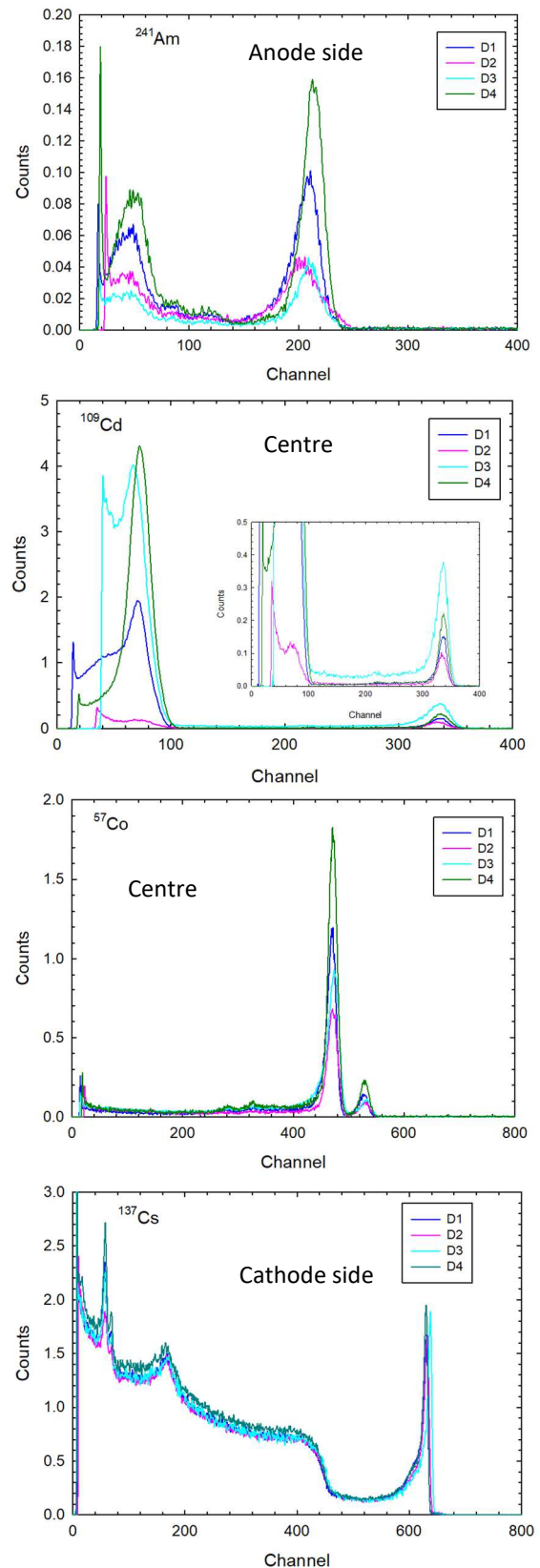


Fig. 9. Spectra acquired irradiating the 4 detectors in PTF at the same energies as in PPF.

The energy resolution values were calculated for all the detectors at the interest energies in both configurations and reported in the following tables.

TABLE III. ENERGY RESOLUTION IN PPF

Energy (keV)	D1 R (%)	D2 R (%)	D3 R (%)	D4 R (%)	Mean (%)
59.54	6.5±0.5	7.8±0.2	6.6±0.1	6.6±0.1	6.9±0.1
88.04	4.2±0.1	5.1±0.2	4.5±0.1	4.7±0.1	4.6±0.1
122.06	3.2±0.1	4.1±0.1	3.4±0.1	3.4±0.1	3.5±0.1
661.67	1.00±0.01	1.21±0.02	1.31±0.05	1.01±0.01	1.12±0.01

TABLE IV. ENERGY RESOLUTION IN PTF MEASURED NEAR THE CATHODE

Energy (keV)	D1 R (%)	D2 R (%)	D3 R (%)	D4 R (%)	Mean (%)
59.54	6.2±0.2	8.4±0.3	7.9±0.3	7.2±0.1	7.4±0.1
88.04	4.5±0.1	5.5±0.1	4.7±0.2	4.7±0.1	4.9±0.1
122.06	3.3±0.1	4.4±0.1	3.6±0.1	3.5±0.1	3.7±0.1
661.67	1.00±0.01	1.18±0.01	1.01±0.01	1.09±0.01	1.07±0.01

The values are quite uniform for 3 out of 4 detectors. In the last column, the mean value shows a good energy resolution with no correction, about 1 % FWHM at 662 keV, confirming the important technological progress in the DSDS fabrication. In addition, the spectral performances are almost equal within the errors in the PTF and PPF configurations.

B. $\mu\tau$ product and Peak to Valley Ratio

A very preliminary analysis shows a good uniformity in terms of electron mobility-lifetime product (see Fig.10) and an improvement in the Peak to Valley ratio at 122 keV in the central position of the PTF configuration with respect to the PPF geometry, as illustrated in Table V.

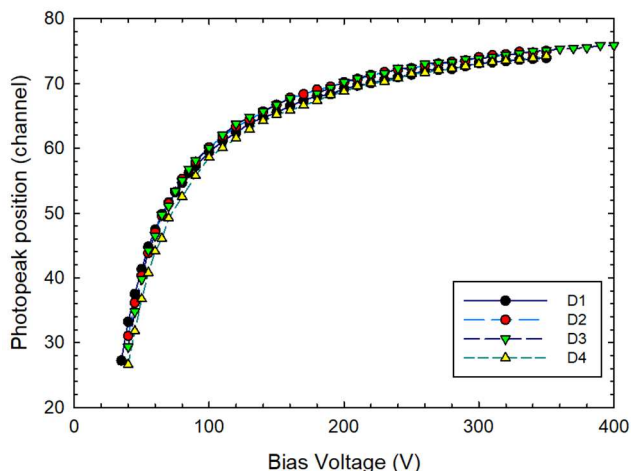


Fig. 10. Charge collection efficiency as a function of the applied voltage at 22 keV of ^{109}Cd . The lines are the best fit with the simplified Hecht equation.

TABLE V. COMPARISON OF THE PEAK TO VALLEY RATIO IN PPF AND PTF CONFIGURATION AT 122 KEV

Detector	P/V in PPF	P/V in PTF (center)
D1	3.3	3.8
D4	3.8	6.7

Further analyses of the data are ongoing to obtain a complete overview of the four detector performances.

C. Threshold

The mean threshold value, measured on the 4 samples, is about 11 keV, as illustrated in Fig. 11 for two strips of two detectors irradiated with a radioactive source of ^{109}Cd .

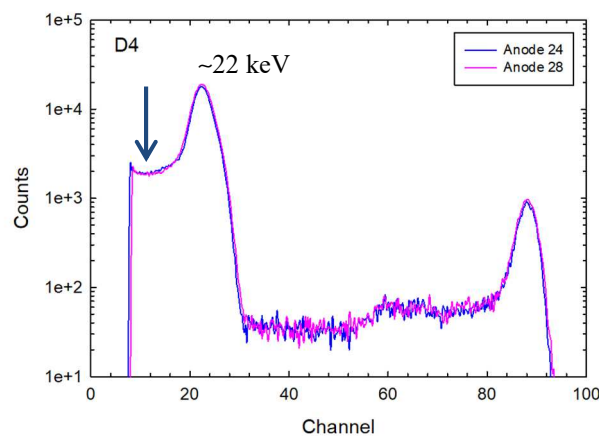
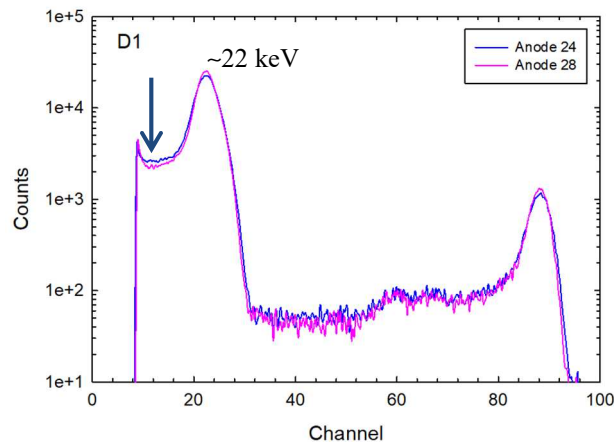


Fig. 11. Energy threshold measured illuminating the D1 and D4 detectors with ^{109}Cd .

D. Scanning in PTF Configuration

Scanning as a function of the position between the anode and the cathode was also performed, in particular at three different positions and different energies. A spectra degradation was observed moving from the cathode to the anode resulting in a shift of the photopeak that means a loss of the collected charge and also a worsening of the energy resolution. In the figure below, the spectra acquired near the cathode, in the center, and near the anode of the detectors D1, D3 and D4 are reported. The positioning was carried out by performing two scans, in X and Y, with steps of 0.25-0.5 and 1 mm in both directions illuminating the detectors through a Pb collimator equipped with a hole of 0.5 mm diameter.

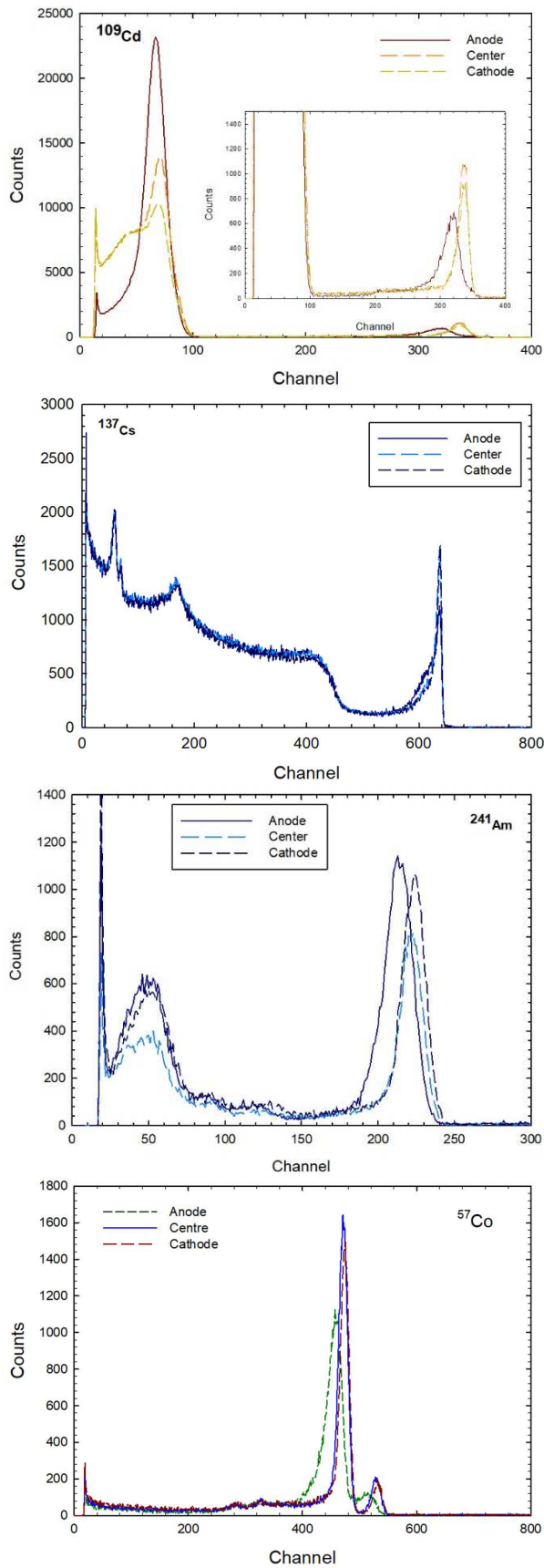


Fig. 12. Spectra acquired at different positions between the electrodes illuminating D1 (top), D2, and D4 (the two spectra in the bottom) with ^{109}Cd , ^{137}Cs , ^{241}Am , and ^{57}Co .

Only three positions are shown.

IX. DETECTOR UNIFORMITY IN PPF AND PTF CONFIGURATION

The uniformity was measured both in PPF and PTF configuration.

In the PPF geometry the linearity of the detection system response, composed by the detector and associated preamplifier chain, is very good in the energy range from 20 keV to 700 keV for all detectors, as illustrated in Fig. 13, in which the fitted photopeak channel is plotted as a function of the energy of the radioactive source lines. Furthermore, the calibration curves are in excellent agreement within the errors.

Fig. 14 reports the percentage deviation of the photopeak channel from the average at the different energies of the used sources for each sensor: the non-uniformity between the detectors is less than 2% for each energy in the energy range from 20 keV to 700 keV excluding the point circled in red.

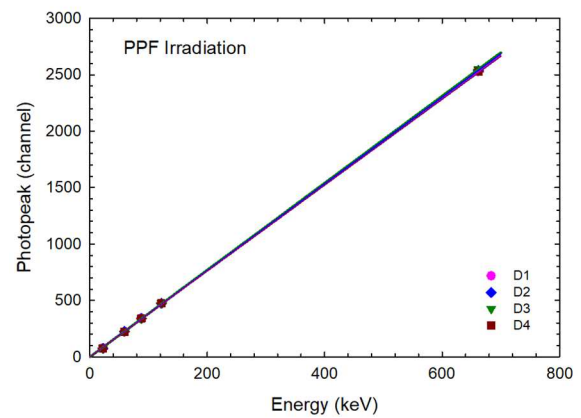


Fig. 13. Linearity vs Energy measured with ^{241}Am , ^{109}Cd , ^{57}Co , and ^{137}Cs in PPF.

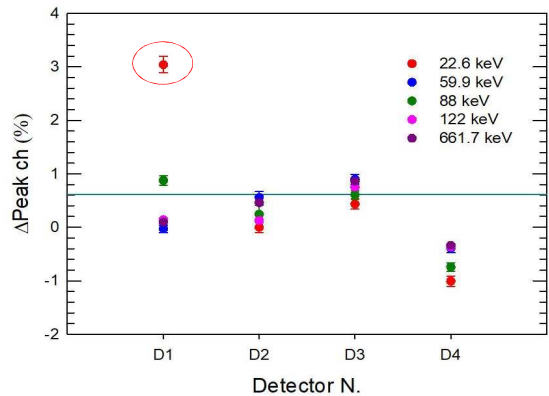


Fig. 14. The Detector Uniformity was measured in PPF with ^{241}Am , ^{109}Cd , ^{57}Co , and ^{137}Cs .

We can infer the same considerations as regards the uniformity in the PTF configuration as the linearity is very good irradiating the detectors in the three positions, already mentioned, between the electrodes that are near the anode, in the center, and near the cathode. The relative plots are displayed in Fig 15. The distributions of the percentage variations ($\Delta\text{Peak}(\%)$) with respect to the average value, at each reference energy, of the peak channel for all the sensors irradiating them in the three positions of the sources used in PTF, are reported in Fig.16.

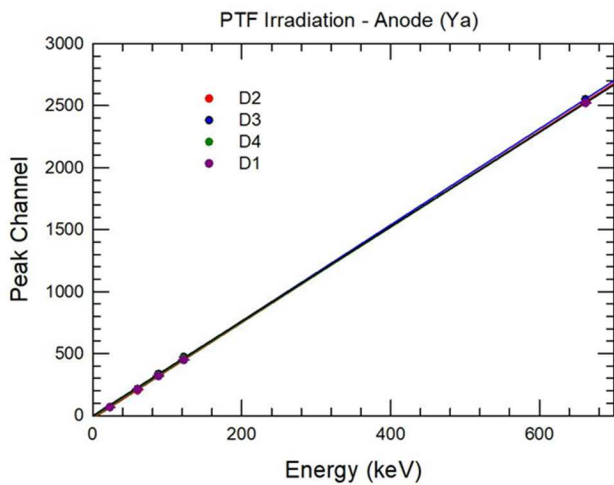
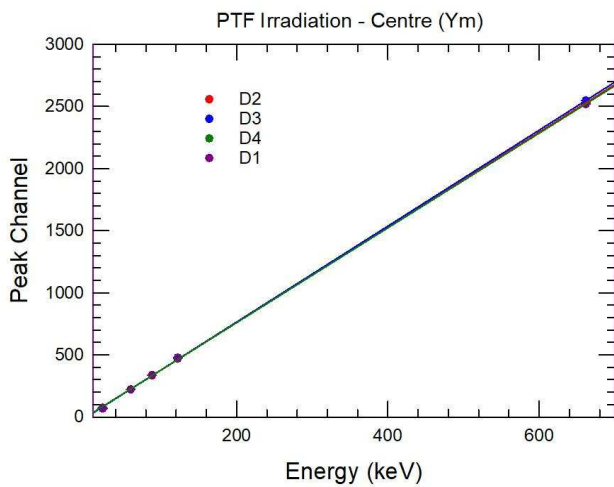
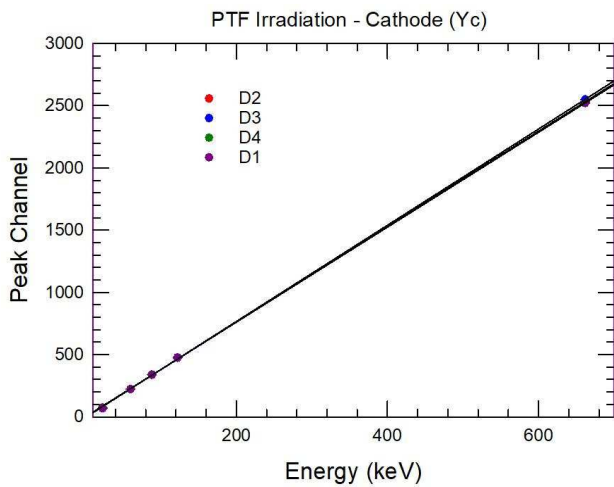


Fig. 15. Linearity vs Energy measured with ^{241}Am , ^{109}Cd , ^{57}Co , and ^{137}Cs in PTF in three different positions.

We can note a significant difference in these distributions, shown below, regarding the gain uniformity as at the anode, the distribution widens and flattens within $\pm 4\%$, while in the other two positions (center and cathode) it remains confined within $\pm 1\%$, even if more spiked for the position near the cathode.

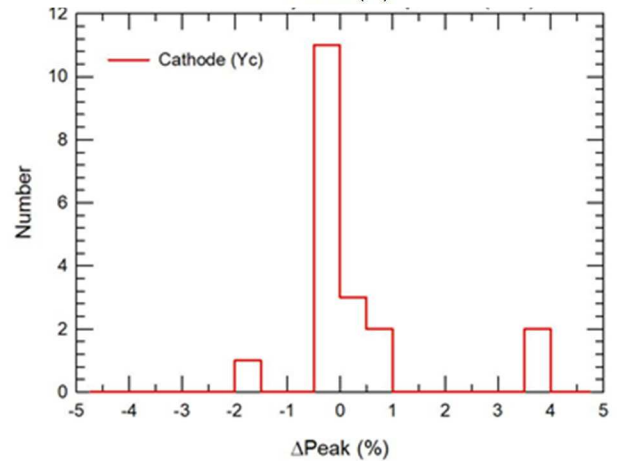
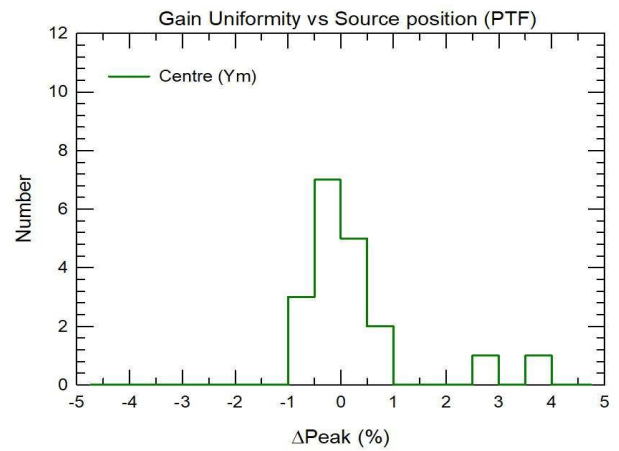
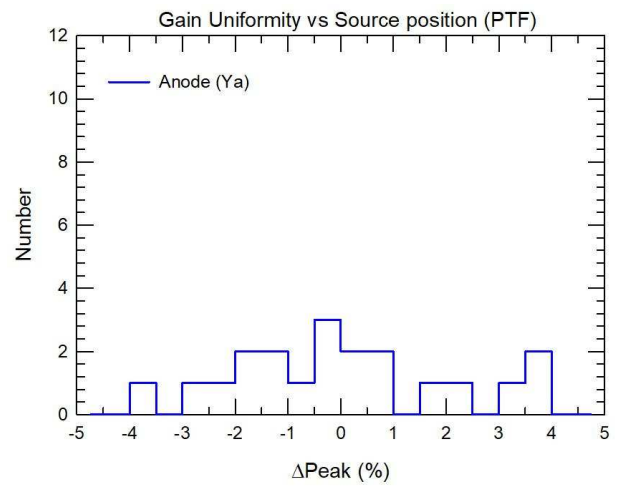


Fig. 16. Uniformity of the gain obtained in PTF configuration.

X. SPECTRA CORRECTION

Eventually, it is worth mentioning a very good result obtained by using custom digital electronics with a dedicated analysis of the pulse shape, height, and coincidence, developed at the University of Palermo and applying a new technique to improve the performances taking into account the negative saturation levels of the induced charge pulses from the drift strip. In Fig. 17 the spectrum acquired with ^{137}Cs at room temperature is shown after correction [5].

The energy resolution FWHM is 0.9% at 662 keV.

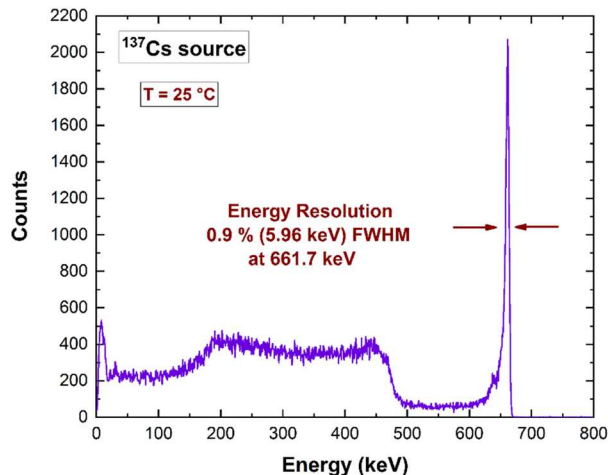


Fig. 17. The corrected spectrum was obtained by implementing a new technique to a ^{137}Cs spectrum acquired by using a signal digital processing.

XI. CONCLUSIONS

We have presented the spectroscopic characterization of 4 detectors of a new CZT Double-Sided Drift Strip prototype with 3D capabilities. Each detector has 24 readout channels: 10 cathodes, 12 anodes and 2 drift strips.

A very good uniformity at room temperature in terms of Charge Collection Efficiency, energy resolution (1.1% FWHM at 662 keV), and electron mobility-lifetime product confirm the technology improvements of the device.

The next steps are the realization of the:

- Charge Sensitive Preamplifier Board based on a Hybrid design and equipped with 16 channels. Its power is 1.4 Watt;
- AFEE board including the detector module, which is composed of 4 detectors, 7 CSP boards, and HV bias circuitry both provided by due2lab s.r.l.

A simplified version of the module, composed of only one detector, will fly onboard a balloon in the framework of the H2020/HEMERA 2nd call from the Esrange base in Kiruna (above the Arctic Circle (68°N , 21°E)) in 2022. This balloon flight opportunity will allow us to perform charged particle background measurement, verify the flexibility of the digital approach in a pseudo space environment and assess the reliability of some technologies, such as the electrode deposition and bonding process. Furthermore, a space application of low cost, low power supply, flexible and large-area devices based on organic semiconductors and Perovskite will be evaluated [6], [7].

ACKNOWLEDGMENT

The current activities are in the framework of two Italian research projects (3DCaTM and 3CaTS projects funded by ASI and INFN, respectively) on the development of spectroscopic gamma-ray imagers (10-1000 keV) for medical and astrophysical applications.

REFERENCES

- [1] He, Z. et al. (1999). *Nucl. Instr. Meth. Phys. Res.*, A 422, 173-178.
- [2] Bolotnikov, A. E. et al. (2020). *Nucl. Instr. Meth. Phys. Res.*, A 954, 161036.
- [3] Budtz-Jørgensen, C. et al. (2017). *IEEE Trans. Nucl. Sci.*, 64, 1611-1618.
- [4] Caroli, E. et al. (2010). *Proceedings of SPIE*, 7742, 77420V.
- [5] Abbene, L. et al. (2020). *J. Synchrotron Rad.*, 27, 1564-1576.
- [6] Basiricò L. et al. (2016), *Nature Communications* 7, 13063.
- [7] Ciavatti A et al. (2019), *Adv. Funct. Mater.* 29, 1902346